Supplementary Material

Insights into electron transfer and bifurcation of the *Synechocystis* sp. PCC6803 hydrogenase reductase module

Elisabeth Lettau[a,b,*,1], **Christian Lorent**[b,1], **Jens Appel**[c], **Marko Boehm**[c], **Paul R. F. Cordero**[a] **and Lars Lauterbach**[a,*]

[a] RWTH Aachen University, iAMB – Institute of Applied Microbiology, Aachen, 52074, Germany
[b] Technische Universität Berlin, Institute for Chemistry, Berlin, 10623, Germany
[c] Universität Kassel, Molecular Plant Physiology, Kassel, 34132, Germany
* corresponding author E-Mail: Elisabeth.lettau@rwth-aachen.de (Elisabeth Lettau), lars.lauterbach@rwth-aachen.de (Lars Lauterbach)
[1] these authors contributed equally to this work

Table S1. Plasmids and primer used in this study.

Plasmid	Description	Reference
pCM66	Addgene plasmid no. 45827 ; kanamycin resistance	[1]
pGE771	pCM62_P_{SH}_StrepTagII-CnhoxFUYHWIhypA2B2F2CDEXABCJ	[2]
pLL71_3	pCM66_P_{SH}_StrepTagII-TEV linker-*CnhoxFU*	This work
pLL293	pCM66_P_{SH}_StrepTagII-*CnhoxFU*	This work
pLL297_91	pCM66_P_{SH}_StrepTagII-*CnhoxF*$^{IA79AC/LASQE119ACGIA}$*U*	This work
pLL9010_40	pCM66_P_{SH}_StrepTagII-*SynhoxEFU*	This work
pLL9079	pCM66_P_{SH}_StrepTagII-*SynhoxFU*	This work
pEL37	pCM66_P_{SH}_*SynhoxE*_StrepTagII-*SynhoxFU*	This work
pEL05	pCM66_P_{SH}_StrepTagII-*SynhoxEF*	This work
pEL06	pCM66_P_{SH}_StrepTagII-*Synhox*E	This work
pEL102	pCM66_P_{SH}_StrepTagII-*SynhoxEFU*^{CTSC192AEQV}	This work
pEL103	pCM66_P_{SH}_StrepTagII-*SynhoxEFU*$^{C192A/C195V/C198A}$	This work
Oligo	Sequence	
880fw	cccgcagttcgaaaaaggcgccatgaccgttgccaccgatcgccaaac	
881rev	gtttggcgatcggtggcaacggtcatggcgccttttttcgaactgcggg	
882rev	caatctcgtctttgtgggggggctcctacctgacccattccttttctttac	
883fw	gtaaagaaaaggaatgggtcaggtaggagccccccacaaagacgagattg	
911fw	gccacccgcagttcgaaaaggcgccatggacattaaagaattaaaggaaattgcc	
912rev	ggcaatttcctttaattctttaatgtccatggcgccttttttcgaactgcgggtggc	
GB009	caaccttggttaagtaacagttaacggtaaggaggagacaccatggctagc	
GB010	cgatcggtggcaacggtcatggtgtctcctccttactaatgttcgcc	
GB011	ggcgaacattagtaaggaggagacaccatgaccgttgccaccgatcg	
GB012	gctagccatggtgtctcctccttaccgttaactgttacttaaccaaggttg	
Q5103F	gccgagcaggtgggcaaatgtgtggatgcctg	
Q5104F	gccacttccgtgggcaaagccgtggatgcctgtcccacgg	
Q5107F	gtaccgagctcgaattcactgg	
Q5109R	gtgtttcagaaaagttaactgagtgg	
Q510R	caactagaaaagatcaagcaatcacc	
Q510xUR	ggcatcaacggttccccagg	

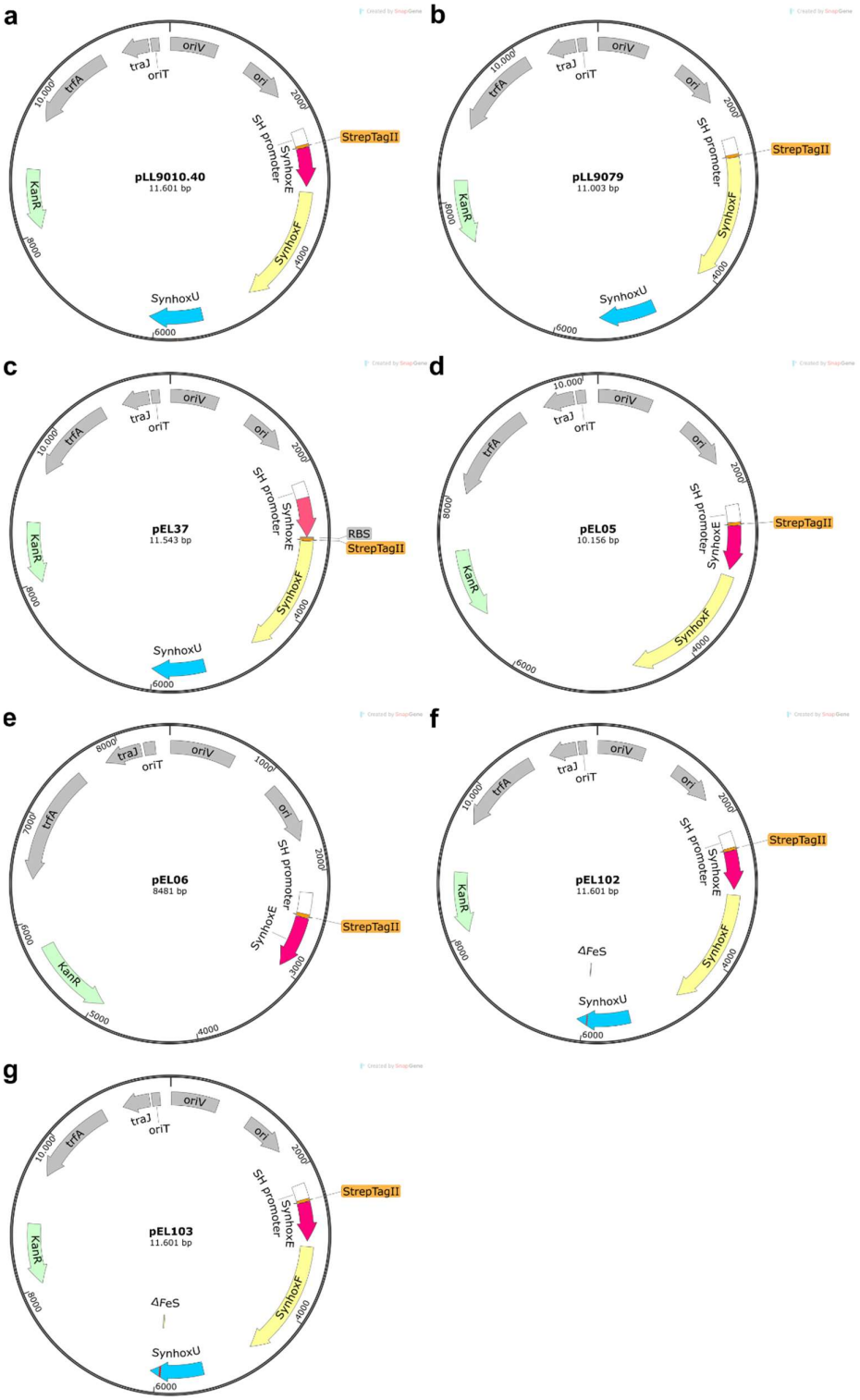

Figure S1. Plasmid maps of reductase derivatives. a) pLL9010.40 used for overproduction of StrepTagII-*Syn*HoxEFU from *Synechocystis* sp. PCC6803. b) pLL9079 used for overproduction of StrepTagII-*Syn*HoxFU. c) pEL37 used for overproduction of *Syn*HoxE+StrepTagII-*Syn*HoxFU. d) pEL05 used for overproduction of StrepTagII-*Syn*HoxEF.e) pEL06 used for overproduction of StrepTagII-*Syn*HoxE. f) pEL102 used for overproduction of StrepTagII-*Syn*HoxEFU^{CTSC192AEQV} (*Syn*HoxEFU$^{\Delta U4a}$). g) pEL103 used for overproduction of StrepTagII-*Syn*HoxEFU^{C192A,C195V,C198A} (*Syn*HoxEFU$^{\Delta U4b}$). Plasmid maps are generated with SnapGene®, GSL Biotech, USA.

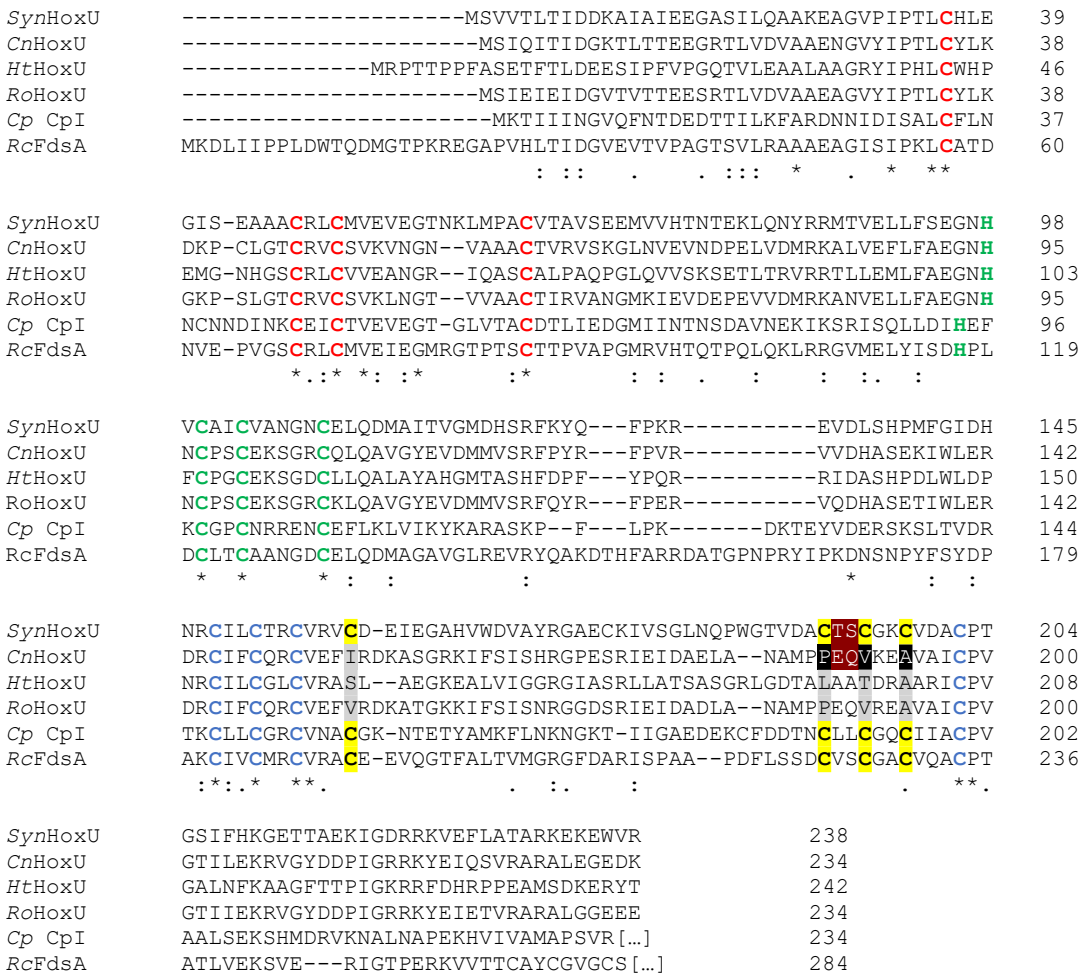

Figure S2. Multiple Sequence alignment of *Synechocystis sp.* PCC6803 HoxU (*Syn*HoxU) with NAD^+-reducing hydrogenase subunit HoxU from *Cupriavidus necator* H16 (*Cn*HoxU), *Hydrogenophilus thermoluteolus* (*Ht*HoxU) and *Rhodococcus opacus* (*Ro*HoxU), as well as FeFe-hydrogenase from *Clostridium pasteurianum* (*Cp*I) and homologous subunit FdsA from *Rhodobacter capsulatus* formate dehydrogenase (*Rc*FdsA). Bolt letters represent the coordinating amino acids for the iron-sulfur clusters. Yellow framed amino acids represent the conserved cysteins coordinating the additional [4Fe4S] cluster U4 in *Syn*HoxU. The grey framed amino acids represend the homologue residues in the bacterial NAD^+-reducing hydrogenases. Amino acids which were substituted to the homologue residues in *Cn*HoxU in the *Syn*HoxFU$^{\Delta U4a}$ and *Syn*HoxFU$^{\Delta U4b}$ derivative in an aim to delete the proposed additional [4Fe4S] cluster U4 in HoxU are framed in dark red and black, respectively.

```
CnHoxF          ------------------MD---SRITTILERYRSDRTRLIDILWDVQHEYGHIPDAVLP   39
TtNqo2          MG-------------FFDDKQDFLEETFAKYPPEGRRAAIMPLLRRVQQEEGWIRPERIE   47
SynHoxE         MTVATDRQTVPPSAAHPSGDKRFKVLDATMKRNQFNQDALIEILHKAQEIFGYLEEDVLL   60
SynHoxF         ------------------------------------------------------------   0
RcFdsG          ----------------MTDT---ARLRAILAAHRGREGALLPILHDVQAAFGFIPEDAYA   41

CnHoxF          QLGAGLKLSPLDIRETASFYHFFLDKPSGKYRIYLCNSVIAKINGYQAVREALERETGIR   99
TtNqo2          EIARLVGTTPTEVMGVASFYSYYQFVPTGKYHLQVCATLSCKLAGAEELWDYLTETLGIG   107
SynHoxE         YVARGLKLPLSRVFGVATFYHLFSLKPSGKHTCVVCLGTACYVKGAGDLLKTLDQEVHLK   120
SynHoxF         ----------MDIKELKEIATKS-REKQTKIRIRCCSAAGCLSSEGETVKKNLT----TA   45
RcFdsG          PIAADLGLTRAEVAGVVGFYHDFRKAPAGRHVIKLCRAEACQAMGMDAVQARLESALGLR   101
                             :    :         :    *    .       :   *

CnHoxF          FGETDPNGMFGLFDTPCIGLSDQEPAMLID--KVVFTRLRPGKIT-DIIAQLKQGRSPAE[…] 156
TtNqo2          PGEVTPDGLFSVQKVECLGSCHTAPVIQVNDEPYV-ECVTRARL-EALLAGLRAGKRLEE[…] 165
SynHoxE         PGETTEDGQMSLVTARCIGACGIAPAVVYDGK--VLGKQNDEAVLAAIQPWLSNS-----   173
SynHoxF         IAAAGLEEKVEVCGVGCMKFCGRGPLVAVDDRNQLYEFVTPDQVG-DIVKKLQKPDAVAE[…] 104
RcFdsG          LGDS--SEAVTLEAVYCLGLCACAPAAMVDDR--LVGRLDAAAVA-GIVAELGA------   150
                 .    .  . :  . *:  .   *    :    :        :   :   *
```

Figure S3. Multiple Sequence alignment of N-terminal *Cupriavidus necator* HoxF (*Cn*HoxF) with *Thermus thermophilus* Complex I subunit Nqo2 (*Tt*Nqo2), Cyanobacterial hydrogenase subunits HoxE and HoxF from S*ynechocystis sp*. PCC6803 (*Syn*HoxE, *Syn*HoxF) and formate dehydrogenase form *Rhodobacter capsulatus* subunit FdsG (*Rc*FdsG). Yellow framed amino acids represent the conserved cysteins coordinating the additional [2Fe2S] cluster in *Tt*Nqo2, *Rc*FdsG, *Syn*HoxE and *Syn*HoxF.

Table S2. Identity of homologues enzymes with *Synechocystis* sp. PCC6803 cyanobacterial hydrogenase. Apart from other cyanobacterial hydrogenases, the *Syn*SH shows highest similarity (highlited in cyan, green, violet) to the electron bifurcating HydABC hydrogenases.

Organism	Enzyme type	Identity to subunit (in percent)				
		HoxH	HoxY	HoxE	HoxF	HoxU
Synechococcus sp. PCC6301	Cyanobacterial SH	70.95	60.33	56.08	59.51	68.91
Hydrogenophilus thermoluteolus	Bacterial SH	45.81	38.6	-	37.43	33.33
Cupriavidus necator H16	Bacterial SH	43.0	41.28	-	36.12	36.16
Rhodococcus opacus	Bacterial SH	42.33	43.02	-	34.87	34.38
Acetomicrobium mobile	NiFe-HydABCSL	53.09 (HydL)	43.65 (HydS)	40.3 (HydC)	55.83 (HydB)	45.41 (HydA)
Thermotoga maritima	FeFe-HydABC	-	-	43.38 (HydC)	47.45 (HydB)	35.61 (HydA)
Clostridium pasteurianum	CpI	-	-	-	-	26.32
Rhodobacter capsulatus	FDH	-	-	32.12 (FdsG)	44.07 (FdsB)	40.43 (FdsA)
Thermus thermophilus	Respiratory Complex I	n.d.	n.d.	31.19 (Nqo2)	46.13 (Nqo1)	n.d.
Escherichia coli	Respiratory Complex I	n.d.	n.d.	28.78 (NuoE)	n.d.	n.d.

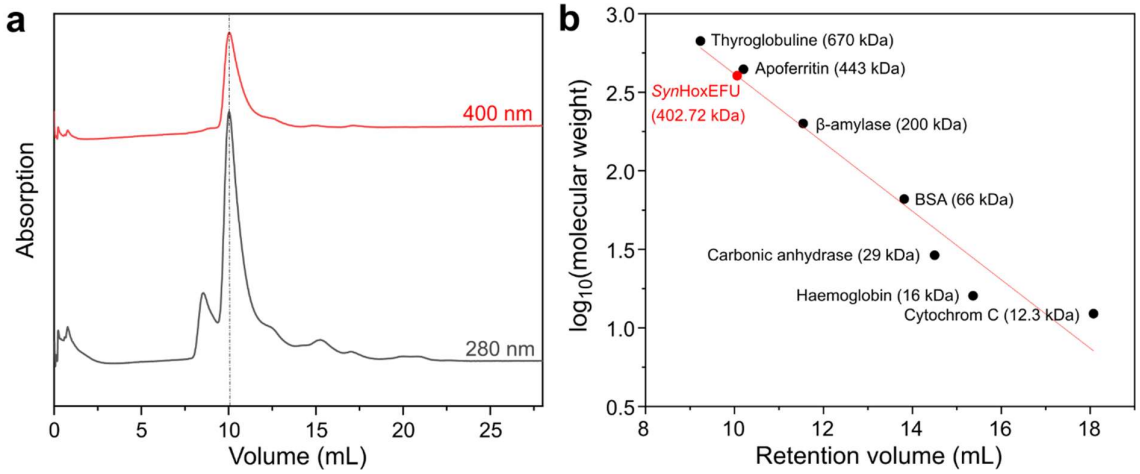

Figure S4. Size exclusion chromatography (SEC) on the isolated *Syn*HoxEFU derivative shows tetramerization of the complex. a) Elution chromatogram of *Syn*HoxEFU at two different wavelengths, 400 nm (red) and 280 nm (grey). Retention volume of *Syn*HoxEFU is around 10 mL (dashed line). b) Calibration curve of standard proteins of different size (black). Retention volume of *Syn*HoxEFU (red) corresponds to a molecular weight of 402.72 kDa, which implicates tetramerization of the complex. This is in contrast to the complete *Syn*SH and other well-characterized NAD^+-reducing hydrogenases for which either monomerization or dimerization has been postulated.[3–6] However, it is in good agreement with the homologous HydABC hydrogenase from *Thermotoga maritima* (*Tm*HydABC), for which tetramerization has also been demonstrated.[7]

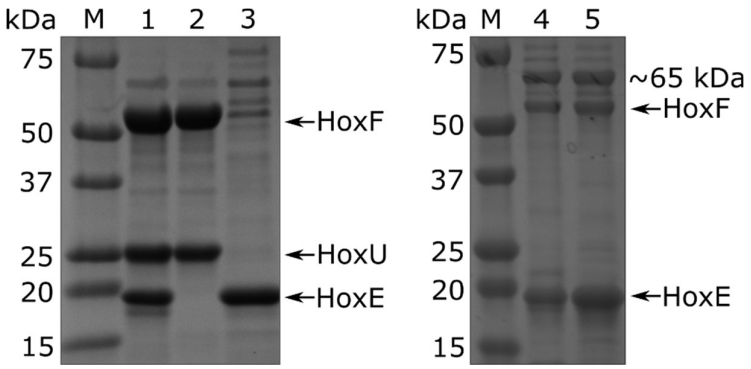

Figure S5. SDS-PAGE of hheterologous produced and purified reductase derivatives from *Synechocystis sp.* PCC6803 in a reductase deficient *C. necator* strain HF903: *Syn*HoxEFU (1), *Syn*HoxFU (2), *Syn*HoxEF (3), *Syn*HoxEFU$^{\Delta U4a}$ (4) and *Syn*HoxEFU$^{\Delta U4b}$ (5); M - protein standard. Whereas the SynHoxEFU und SynHoxFU derivatives could be purified in good yield and purity, the deletion of the HoxU subunit in the *Syn*HoxEF derivative resulted in low purity and yield. Only 30 µg from one g cell pellet (wet weight) could be purified. It also leads to a sub-stoichiometric amount of HoxF in comparison to HoxE. In the SDS-PAGE gel, only a narrow band with the appropriate size for HoxF can be observed, whereas as a prominent band for HoxE is visible. The deletion of the supposed additional [4Fe4S] cluster in HoxU resulted in a loss of HoxU in both variants HoxEFU$^{\Delta U4a}$ and HoxEFU$^{\Delta U4b}$ together with low yield and purity of purified protein. An average of only 26 µg could be purified from one g cell pellet (wet weight) in both cases. In the SDS-PAGE gel, only corresponding bands for HoxE and F could be identified. Furthermore, in both SDS-PAGE gels, for the *Syn*HoxEF derivative and the both *Syn*HoxEFU$^{\Delta U4}$ variants, an additional band of approximately 65 kDa is visible, which typically appears with *Strep*Tag purified unstable hydrogenase derivates and was previously identified as homologue of heat shock protein DnaK.[8]

Table S3. Iron and FMN incorporation of heterologous produced reductase derivatives. Iron content was analyzed by ICP-OES spectrometry and FMN content by protein precipitation and photometry. The respective protein concentration was determined with a BCA assay, which may cause protein overestimation.[9] It is noticeable that the respective cofactor saturation is strongly dependent on the respective batch. At least two technical replicates of two biological replicates were examined.

	Iron content [%]	FMN per molecule
*Syn*HoxEFU	61 ± 12	0.63 ± 0.17
*Syn*HoxFU	30 ± 3	0.7 ± 0.1
*Syn*HoxE	41± 6	n. d.

Development of a kinetic assay for the investigation of oxidoreductase activity

To demonstrate the functionality of the purified reductase derivatives we performed kinetic measurements based on the NAD(P)H oxidoreductase activity. Because the hydrogenase active site is missing in the reductase derivatives we used redox dyes as artificial electron acceptor as readout to perform photometrical activity measurements. Different redox dyes were tested to achieve the highest possible activities (Figure S6, panel A). Benzyl viologen and methylene blue was used previously to demonstrate the *C. necator* and *Synechocystis* reductase NADH oxidation activity, respectively.[10,11] Only low activity could be measured using benzyl viologen as artificial electron acceptor, 5.9 ± 0.7 min^{-1} and 3.3 ± 1.4 min^{-1} for NADH and NADPH, respectively. It was not possible to determine NADH oxidation activity, using methylene blue as electron acceptor, because we observed a strong non-enzymatic reduction after addition of 1 mM NADH to the reaction mixture, also when no enzyme was added (Figure S6, panel B), which suggests direct electron transfer from NADH to methylene blue.[12,13] When ferricyanide was used as artificial electron acceptor we were able to measure higher activities of 232 ± 43 min^{-1} and 262 ± 7 min^{-1} for NADH and NADPH, respectively. However, ferricyanide tends to instability in solution, which resulted in a high variability of the determined activities. Despite its unsuitable redox potential for NADH oxidation (MV: E^0 = - 446 mV, $NADH/NAD^+$: E^0 = -320 mV versus NHE), the highest activities were observed when methyl viologen was used as electron acceptor probably due to its small molecule size and charge. A NADH reduction activity of 3155 ± 400 min^{-1} could be measured, whereas NADPH oxidation activity was not detectable using methyl viologen as electron acceptor, even by using really high amounts of NADPH up to 2 mM. This phenomenon probably can be attributed to a combinatory effect of the unfavorable redox potential of methyl viologen and the approximately 25-fold lower affinity of *Syn*SH for NADPH compared to NADH.[11,14–16] As previous studies have extensively explored the cofactor dependency of the *Synechocystis* hydrogenase, we only focus on NADH turnover activity here.[11,16] All further activity measurements were carried out by using methyl viologen as artificial electron acceptor. Since the cofactor analyses showed that the purified reductase derivatives are not fully loaded with their cofactors we investigated if an *in vitro* reconstitution of FMN could further rise the activity. Neither addition of 1 µM FMN nor 1 mM dithiothreitol (DTT) has any effect to the activity in contrast to previous observations on *Cn*SH (Figure S6, panel C).[17,18] To determine optimal assay conditions the NADH oxidoreductase activity was determined at temperatures ranging from 5°C to 70°C. Highest activity was reached at 45°C to 50°C (Figure S7, panel A), concordant with previous results, where the temperature optimum of *Syn*SH was found to be 60°C, at pH 6.3.[3] However, NADH-oxidation activity diminished significantly after a short time at temperatures above 40°C, indicating protein instability. Therefore, we decided to perform all further measurements at 35°C. Furthermore, oxidoreductase activity was determined at pH values ranging from 5.5 to 10.0 in a broad range buffer system. Highest activity was reached at pH 8.5 (Figure S7, panel B). Since, pH 8.5 is slightly above the buffer capacity of potassium phosphate buffer, we performed the measurements for the kinetic characterization of the reductase derivatives at pH 8.0. Usage of a tris-base buffer system resulted in a yellow coloring of the reaction mixture, indicating the formation of methyl viologen radicals and was therefore not suitable for this assay. In order to compare the reductase derivatives with each other, all subsequent kinetic studies were carried out in potassium phosphate buffer pH 8.0 at 35°C.

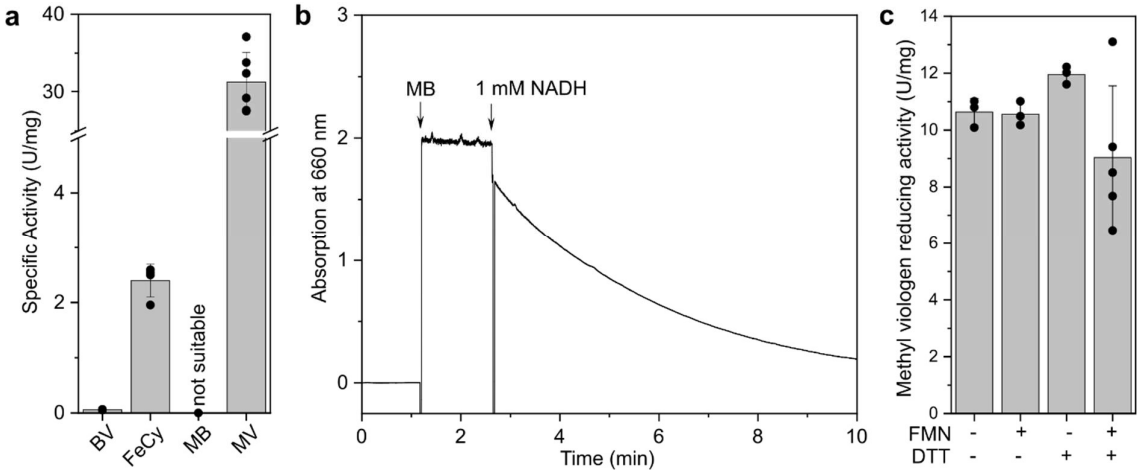

Figure S6. Investigation of suiteable artifical electron aceptors for NADH dependent photomerical acativity measurements. a) Specific activity of NADH dependent reduction of different artifical electron aceptors: benzyl viologen (BV), ferricyanide (FeCy), methylene blue (MB) and methyl viologen (MV). b) Enzyme independent reduction of methylene blue by NADH in 50 mM Tris/HCl buffer pH 8.0. Methylene blue is directly reduced after addition of 1 mM NADH without any enzyme. c) Influence of reconstitution with flavin mononucleotide (FMN) and/or dithiotreithiol (DTT) in NADH::MV oxidoreductase activity of HoxEFU. At least three technical replicates (dots) where examined, error bars indicate standard deviation.

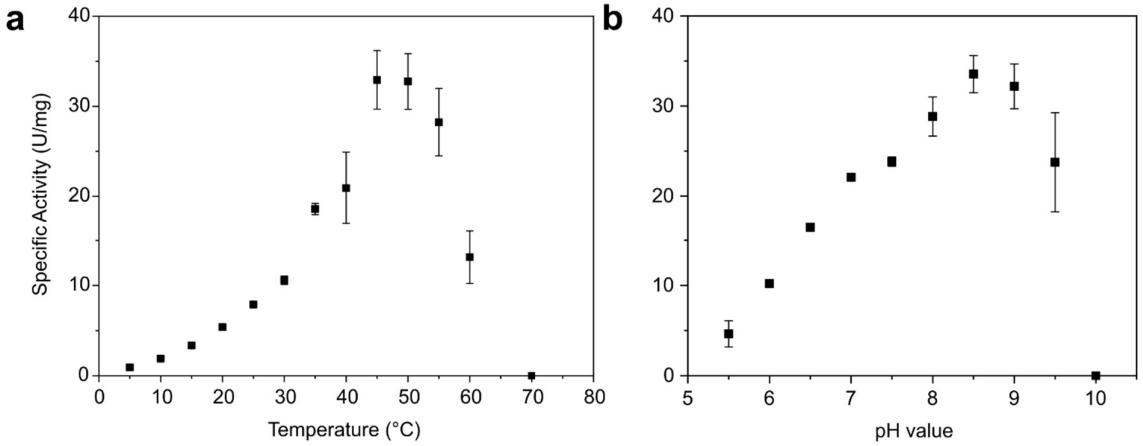

Figure S7. Determination of optimal assay conditions for NADH dependent MV reduction activity measurement. a) Determination of the temperature optimum at 45 to 50°C. b) Determination of pH optimum at pH 8.5. In contrast to all other meassurements, which were carried out in potassium phosphate buffer pH 8.0, the pH dependency was determind in a broad-range CTG buffer. Three technical replicates were examined, error bars indicate standard deviation.

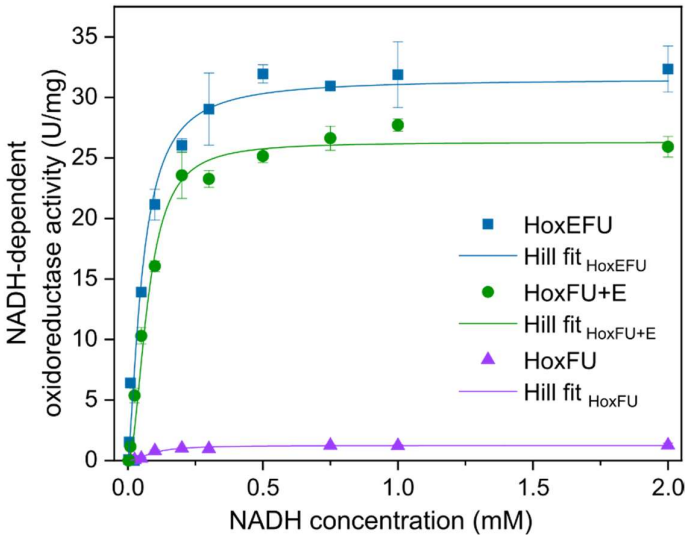

Figure S8. Kinetic fits for NADH dependent MV reduction of the *Synechocystis* reductase HoxEFU, HoxFU and HoxFU+E. For determination of kinetic parameters of HoxEFU a Hill fit was used. For the HoxFU derivative a substrat inhibition model was used and the HoxFU+E reconstitution was fitted with a biexponential Hill fit.

Table S4. Kinetic parameters for NADH-oxidoreductase activity of *Synechocystis* reductase derivatives

	K' (µM)	n	v_{max} (µmol min^{-1} mg^{-1})	k_{cat} (s^{-1})
HoxEFU	54 ± 14	1.45	32 ± 2	53 ± 7
HoxFU	92 ± 13	1.94	1.24 ± 0.06	1.7 ± 0.1
HoxFU+E	74 ± 9	2.0	26 ± 1	31 ± 2

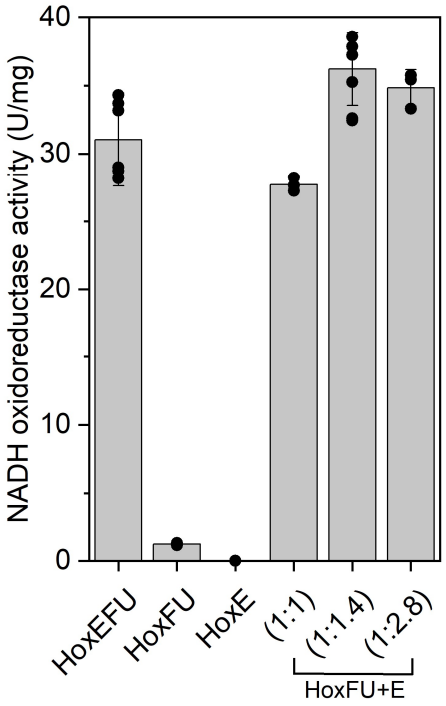

Figure S9. Influence on HoxFU to HoxE ratio on reductase activity. Error bars indicate standard deviation of at least three technical replicates, represented as dots.

Table S5. Ferredoxin dependent NAD^+ reducing activity of reductase derivatives from *Synechocystis* and SH variations from *C. necator*

Enzyme	**Fdx_{red}::NAD^+ reducing activity (mU mg^{-1})**
*Syn*HoxEFU	25.07 ± 1.33
*Syn*HoxFU	1.37 ± 0.08
*Syn*HoxFU+E	12.00 ± 0.53
*Cn*SH	2.68 ± 0.41
CnSH^{+2Fe2S}	1.74 ± 0.35
*Syn*HoxEFU w/o Fdx	3.31 ± 0.60
BSA	1.20 ± 0.99

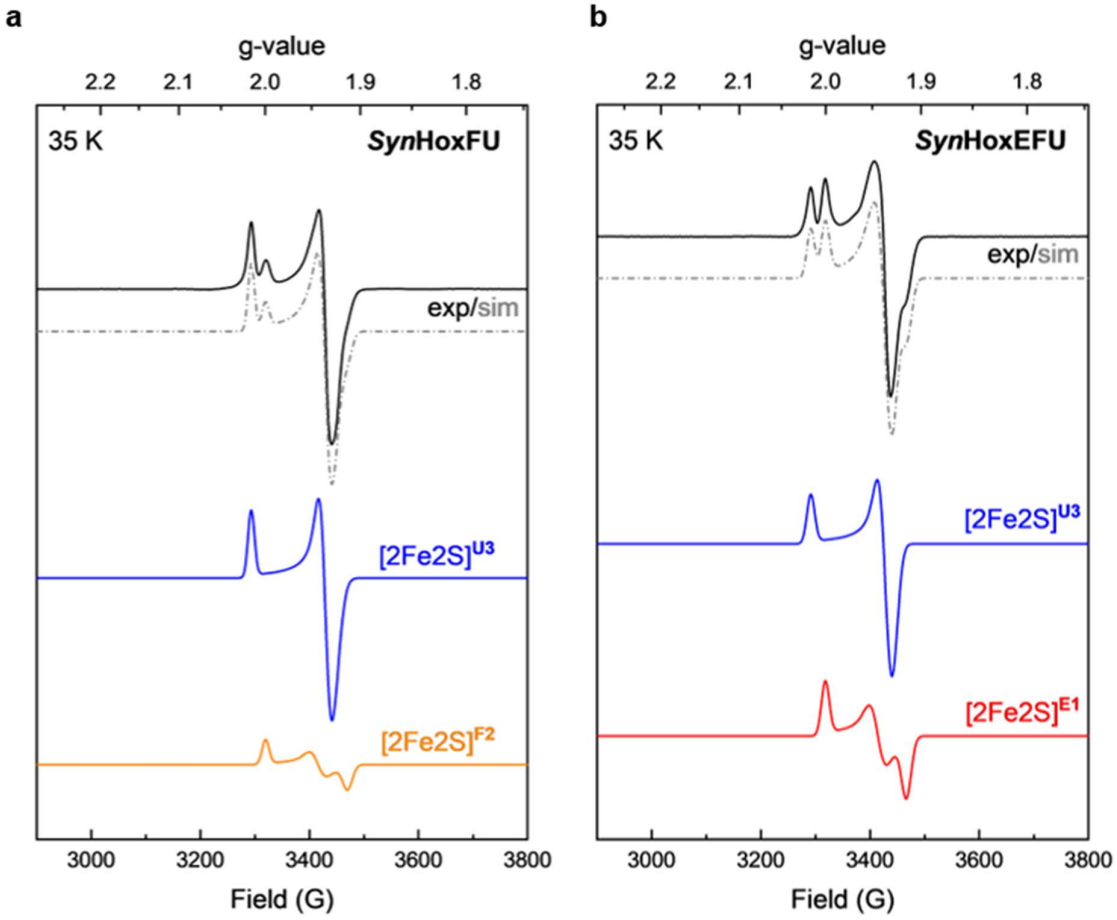

Figure S10. Numerical simulation of the [2Fe2S] cluster signals in the EPR spectra of NaDT-reduced *Syn*HoxFU (a) and *Syn*HoxEFU (b). The experimental spectrum is displayed as black, the simulated spectrum as grey dotted/dashed line. Signals assigned to the [2Fe2S] clusters are respectively labelled in red (E1), blue (U3) and orange (F2).

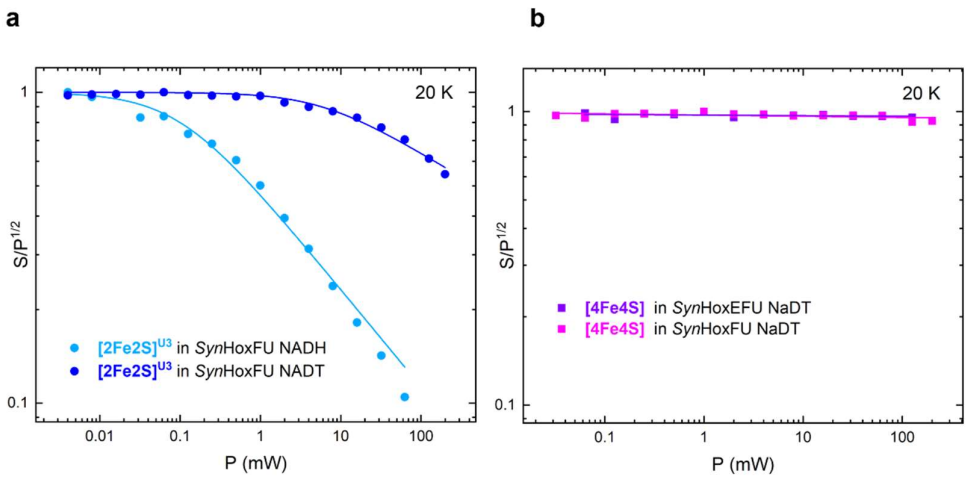

Figure S11. Power saturation of $[2Fe2S]^{U3}$ in *Syn*HoxFU after NADH in light blue and NaDT reduction in blue (c) and of [4Fe4S] cluster(s) in NaDT-reduced *Syn*HoxFU in purple and *Syn*HoxEFU in magenta (d). The signals from the [4Fe4S] cluster(s), measured at g = 1.88, remain unsaturated at 20 K over a broad range of power, which is characteristic for these metal sites, as they usually undergo significantly faster spin relaxation compared to [2Fe2S] clusters.[19] Details for the power saturation are listed in Table S6.

Table S6. Power saturation data of the [2Fe2S] clusters recorded at 20 K.

Protein	Cluster	Redox treatment	Signal/g-value*	$P_{1/2}$ [mW]	b
*Syn*HoxE	E1	NaDT	1.945	0.54	1.21
*Syn*HoxFU	F2	NaDT	2.001	0.30	0.70
*Syn*HoxEFU	E1	NaDT	2.002	0.45	1.11
*Syn*HoxFU	U3	NADH	1.939	0.01	0.62
*Syn*HoxFU	U3	NaDT	1.939	5.93	0.31

* g-component from which the power-dependent intensity was measured

The normalized experimental data was fitted to the empirical equation, that describes the expected saturation behavior. S is the intensity of the respective signal, $P^{1/2}$ is the power of half-saturation and b a parameter related to inhomogeneous ($b \approx 1$) or homogenous ($1 > b > 3$) line broadening. A value for b significantly below 1 indicates dipolar coupling.[20,21]

Table S7. Observed and previously reported g-values of the [2Fe2S] clusters and homologues.

Protein	Subunit/Nickname	g_x	g_y	g_z	References
*Syn*HoxE	E1	2.002	1.945	1.915	This work*
*Syn*HoxFU	F2	2.001	1.945	1.915	This work*
E. coli complex I	NuoE/N1a	2.00	1.94	1.92	[22]
bovine complex I	24 kDa subunit/N1a	2.004	1.945	1.917	[23]
P. denitrificans complex I	25 kDa subunit NQO2	2.00	1.95	1.92	[24]
HydABC from *T. maritima*	HydB	2.003	1.953	1.923	[7]
FDH from *R. capsulatus*	G7	2.002	1.946	1.917	[25]
*Syn*HoxEFU	U3	2.017	1.939	1.929	This work[#11,26]
*Ht*SH	U3	2.026	1.935	1.935	[27]
SH from *A. variabilis*	not assigned	2.021	1.94	1.935	[28]
*Pf*SHI	γ	2.03	1.93	1.92	[29]
E. coli complex I	NuoG/N1b	2.03	1.94	1.94	[22]
bovine complex I	75 kDa subunit/N1b	2.024	1.941	1.926	[23]
FDH from *R. capsulatus*	A5	2.021	1.943	1.941	[25]

* A signal at g = 2.002 respectively g_x = 1.998, g_y = 1.945 and g_z = 1.913 has been observed by Germer et al. and Artz et al., but not assigned to a specific cluster.[11,26]

[#] A signal at g_x = 2.016, g_y = 1.935 and g_z = 1.928 respectively g_x = 2.016, g_y = 1.939 and g_z = 1.929 has been observed by Germer et al. and Artz et al., but not assigned to a specific cluster.[11,26]

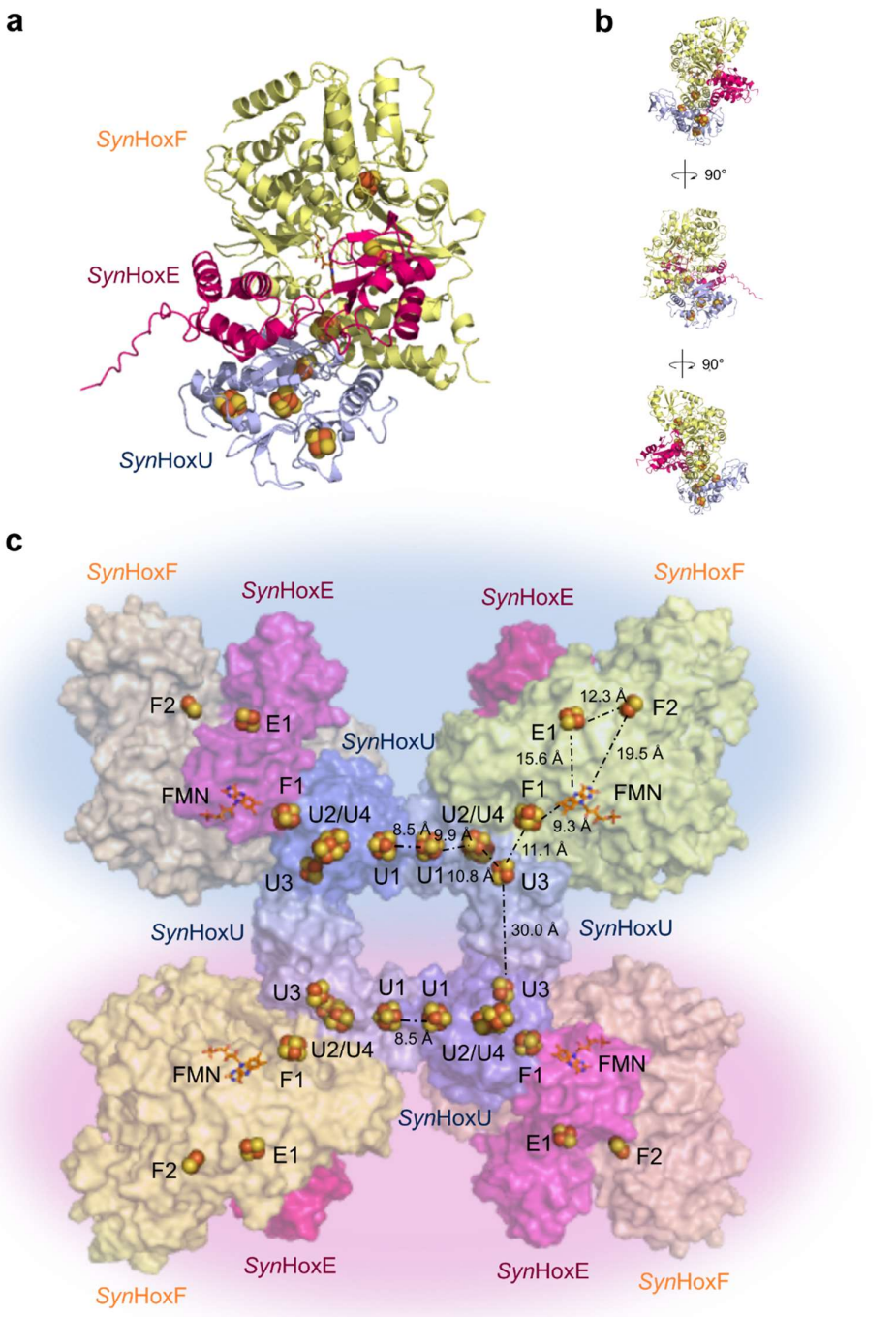

Figure S12. Predicted AlphaFold[30,31] structure of SynHoxEFU (a). Cofactors were inserted with the AlphaFill algorithm.[32] b) All-around views of the structural model rotated by 90°. c) Homology model of *Syn*Hox(EFU)$_4$ tetramer based on *Tm*HydABC (PDB: 7p5h) was built with SWISS-Model (QMEANDisCo global value 0.70 ± 0.05).[33] Relationships and distances of the cofactors are indicated. Each two of the four units are electrically coupled via [4Fe4S]^{U1} cluster, thus giving explanation for the positive cooperativity detected by our kinetic studies. Snapshots of the structure models were obtained using PyMOL.[34]

Table S8. Distances between cofactors homologues to those in SynHoxEFU. *The distances of the cofactors in *Syn*HoxEFU, *Sa*HydAB and *Sw*HydABC were determined using the AlphaFold models, where respective cofactors were inserted into using the AlphaFill algorithm. As a comparison, we used the experimentally determined structures of the BF hydrogenases from *Thermotoga maritima* (*Tm*HydABC) (PDB: 7p5h) and *Acetomicrobium mobile* (*Am*HydABCSL) (PDB: 7t30) and the non-BF enzymes: SH from *Hydrogenophilus thermoluteolus* (*Ht*SH) (PDB: 5xf9), [FeFe] hydrogenase I from *Clostridium pasteurianum* (CpI) (PDB: 1feh), respiratory complex I from *Thermus thermophilus* (*Tt*RC I) (PDB: 3iam) and formate dehydrogenase from *Rhodobacter capsulatus* (*Rc*FDH) (PDB: 6tga).

Respective cofactor pair in SynHoxEFU	Distances between cofactors (Å)								References
	F2-E1	E1-FMN	F2-FMN	FMN-F1	F1-U3	U3-U2	U2-U1	U2-U4	
*Syn*HoxEFU*	12.3	15.6	19.5	9.3	11.1	10.8	9.9	8.5	This work
*Tm*HydABC	12.0	15.6	20.1	6.8	10.1	12.8	7.9	9.2	[7]
*Am*HydABCSL	12.3	15.0	n.i.	n.i	13.7	13.3	11.9	12.1	[6]
*Sa*HydAB*	-	11.7	-	10.9	12.7	10.4	10.6	9.1	This work
*Sw*HYDABC*	-	13.9	-	10.6	11.9	10.6	10.6	9.1	This work
*Ht*SH	-	-	-	12.3	13.7	13.5	12.1	-	[5]
CpI	-	-	-	-	-	13.7	12.2	12.3	[35]
*Tt*RC I	-	15.9	-	12.2	13.8	10.0	12.3	-	[36]
*Rc*FDH	-	15.1	-	12.6	13.8	14.0	12.1	11.8	[37]

Binding Model of *Syn*PetF with the *Synechocystis* Hydrogenase reveals two potential binding sites

Docking models of *Syn*PetF (PDB: 1off)[38] and a calculated *Syn*SH structure were generated using HDOCK.[39–41] Within the top 10 models, three possible interaction regions were calculated, all located at the reductase module. After eliminating all models that do not allow appropriate electron transfer between the iron-sulfur cluster of PetF and an iron-sulfur cluster of *Syn*SH, two possible binding sites remain (Figure S13, panel A).[42] The probability that ferredoxin binds to these two sites is only in the possible range based on confidence scores of 0.634 and 0.589, respectively.[40] However, none of the other docking models had a higher confidence score. The low confidence scores are consistent with the fact that measuring PetF interaction with the *Syn*SH is really challenging and, moreover, with the observation that ferredoxin only binds briefly also to its close relative *Am*HydABCSL.[6] As expected, one of the two possible binding sites is on HoxF with a possible electron transfer to the $[2Fe2S]^{F2}$ cluster. Actually, the distance between the iron-sulfur cluster in PetF and the $[2Fe2S]^{F2}$ cluster in HoxF is 17.3 Å, which is slightly too large for efficient electron transfer. But, a tyrosine (Tyr117) in HoxF between the ferredoxin docking region and the F2 cluster could take on a tunneling function.[43,44] This reduces the transfer distances to 12.6 Å and 6.8 Å respectively, which would allow efficient electron transfer (Figure S13, panel B).[42] The second possible binding site for PetF is on the HoxU subunit, where electron transfer would be possible via the $[4Fe4S]^{U4}$ cluster. The distance between the two iron-sulfur clusters is about 15.1 Å.

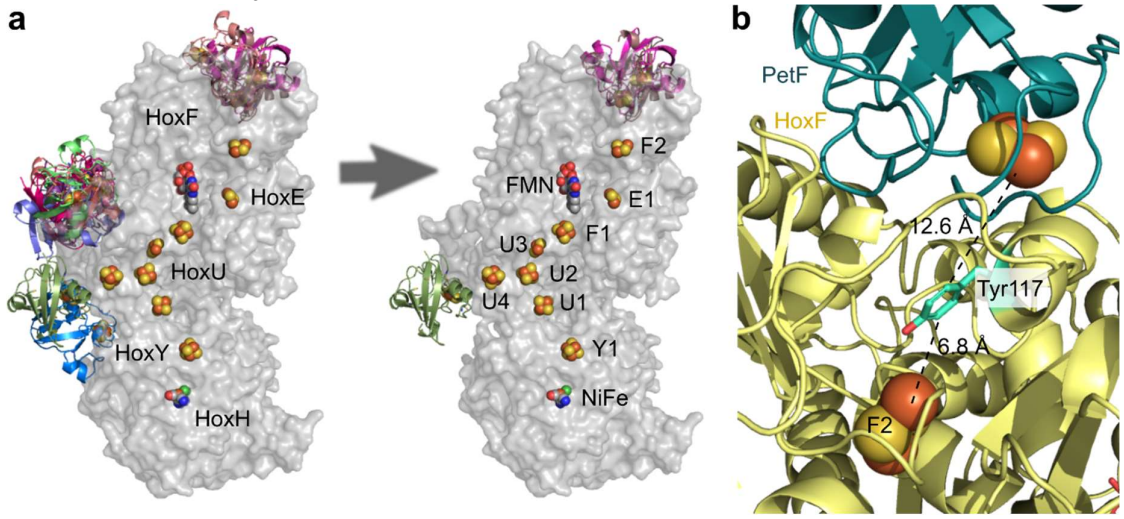

Figure S13. Binding model of PetF and *Synechocystis* hydrogenase. a) Docking models calculated by HDOCK revel two potential bind-ing sites for PetF. One at HoxF and one at HoxU, where either the iron-sulfur cluster F2 or U4 can act as electron acceptors. b) Tyrosine 117 can take an electron tunneling function to allow efficient electron transfer from PetF to the F2 [2Fe2S] cluster in HoxF.

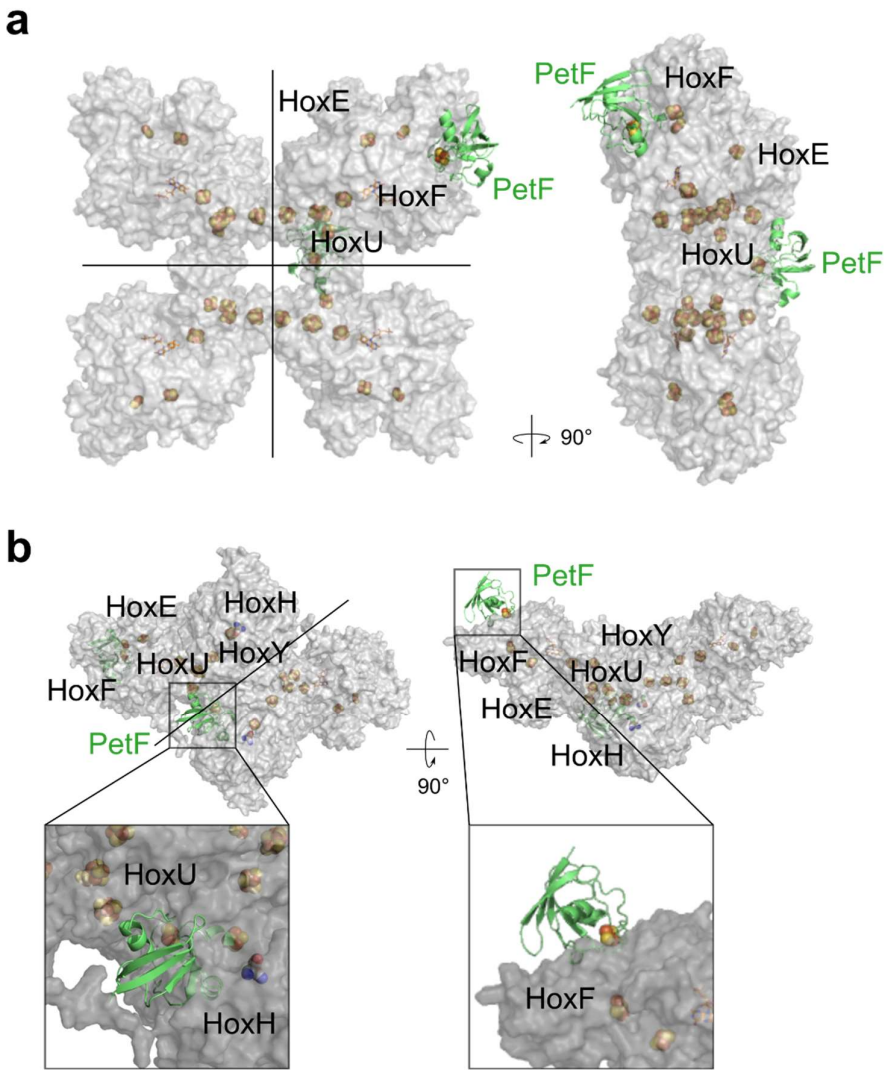

Figure S14. Binding of PetF on oligomeric *Syn*SH variants. a) Both potential binding sites for PetF on HoxF and HoxU are accessible in the *Syn*Hox(EFU)$_4$ tetramer. b) But in the *Syn*(SH)$_2$ the potential binding site at HoxU is blocked by the HoxH subunit of the second SH molecule.

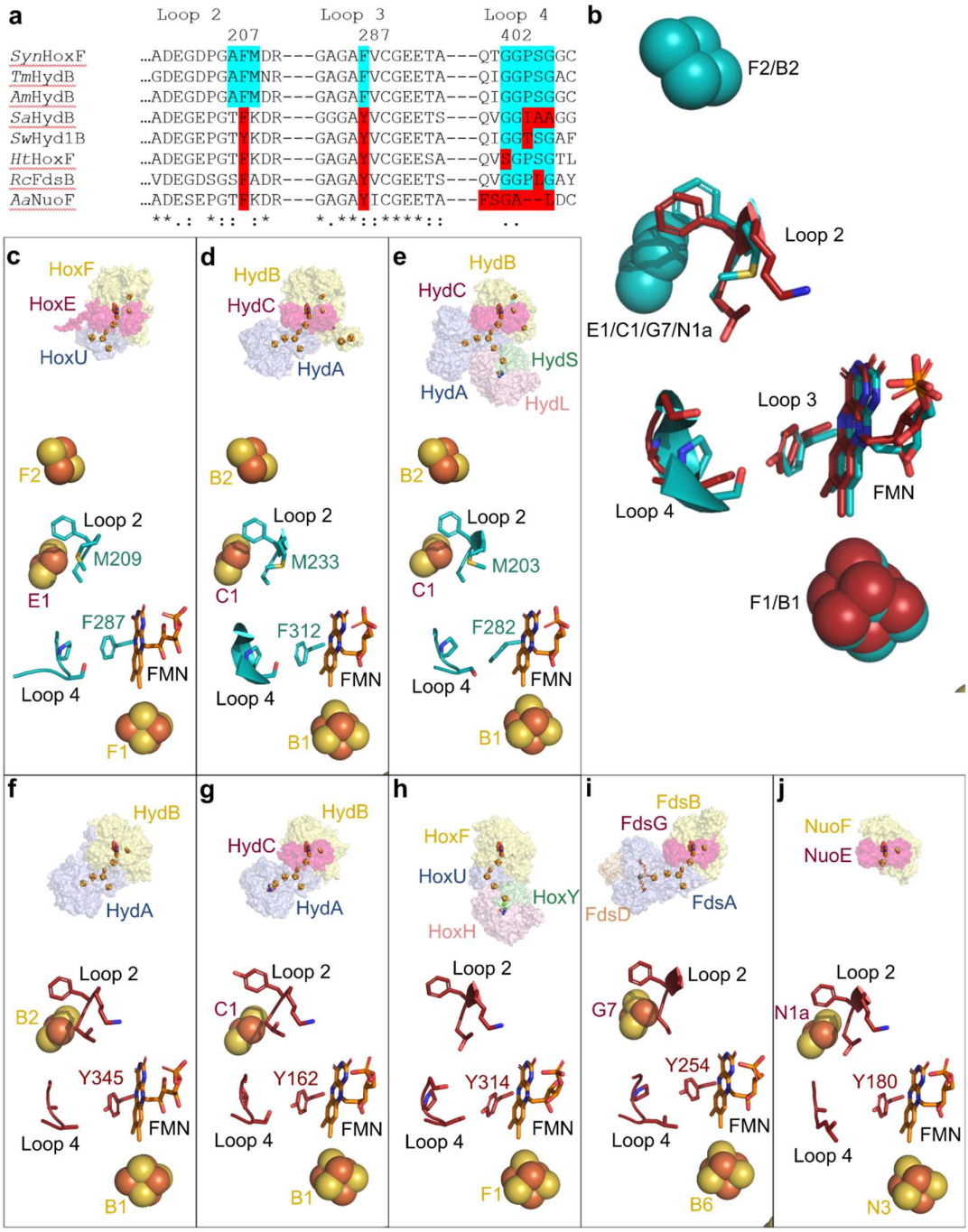

Figure S15. Alignment of SynHoxF and homologous subunits of BF and non-BF enzymes. a) Sequence alignment of the FMN coordinating Rossmann fold loop two, three and four of *Synechocystis* HoxF (*Syn*HoxF), *T. maritima* HydB (*Tm*HydB), *A. mobile* HydB (*Am*HydB), *S. acidotrophicus* HydB (*Sa*HydB), *S. wulferi* HydB (*Sw*Hyd1B), *H. thermophilus* HoxF (*Ht*HoxF), *R. capsulatus* FdsB (*Rc*FdsB) and *A. aquifex* NuoF (*Aa*NuoF). Conserved residues of BF enzymes are highlighted in cyan and deviating amino acids in non-BF enzymes are highlighted in red. b) Superposition of loops two, three and four of the FMN-coordinating Rossmann fold of BF hydrogenase from *T. maritima* (cyan) and non-BF hydrogenase from *H. thermophilus* (red). Structure of the FMN binding pocket from c) *Synechocystis** d) *T. maritima* (PDB:7p8n), e) *A. mobile* (PDB7t2r), f) *S. acidotrophicus**, g) *S. wulferi* *, h) *H. thermoluteolus* (PDB: 5xf9), i) *R. capsulatus* (PDB: 6tg9) and j) *A. aquifex* (PDB: 6hl2). Asterisk indicates AlphaFold predicted structures.

References

1. Marx, C. J. & Lidstrom, M. E. Development of improved versatile broad-host-range vectors for use in methylotrophs and other gram-negative bacteria. *Microbiology (N Y)* **147**, 2065–2075 (2001).
2. Lauterbach, L. & Lenz, O. Catalytic production of hydrogen peroxide and water by oxygen-tolerant [NiFe]-hydrogenase during H_2 cycling in the presence of O_2. *JACS* **135**, 17897–17905 (2013).
3. Schmitz, O. *et al.* HoxE - A subunit specific for the pentameric bidirectional hydrogenase complex (HoxEFUYH) of cyanobacteria. *Biochem. Biophys. Acta - Bioenerg.* **1554**, 66–74 (2002).
4. Eckert, C. *et al.* Genetic analysis of the Hox hydrogenase in the cyanobacterium *Synechocystis* sp. PCC 6803 reveals subunit roles in association, assembly, maturation, and function. *JBC* **287**, 43502–43515 (2012).
5. Shomura, Y. *et al.* Structural basis of the redox switches in the NAD^+-reducing soluble [NiFe]-hydrogenase. *Science (1979)* **357**, 928–932 (2017).
6. Feng, X., Schut, G. J., Haja, D. K., Adams, M. W. W. & Li, H. Structure and electron transfer pathways of an electron-bifurcating NiFe-hydrogenase. *Sci. Adv.* **8**, 7546 (2022).
7. Furlan, C. *et al.* Structural insight on the mechanism of an electron-bifurcating [FeFe] hydrogenase. *Elife* **11**, 1–20 (2022).
8. Jones, A. K., Lenz, O., Strack, A., Buhrke, T. & Friedrich, B. NiFe hydrogenase active site biosynthesis: Identification of Hyp protein complexes in *Ralstonia eutropha*. *Biochem.* **43**, 13467–13477 (2004).
9. Albracht, S. P. J., Van Der Linden, E. & Faber, B. W. Quantitative amino acid analysis of bovine NADH:ubiquinone oxidoreductase (Complex I) and related enzymes. Consequences for the number of prosthetic groups. *Biochim. Biophys. Acta - Bioenerg.* **1557**, 41–49 (2003).
10. Lauterbach, L., Idris, Z., Vincent, K. A. & Lenz, O. Catalytic properties of the isolated diaphorase fragment of the NAD^+-reducing [NiFe]-hydrogenase from *Ralstonia eutropha*. *PLoS One* **6**, (2011).
11. Artz, J. H. *et al.* The structure and reactivity of the HoxEFU complex from the cyanobacterium *Synechocystis* sp. PCC 6803. *JBC* **295**, 9445–9454 (2020).
12. Atamna, H. *et al.* Methylene blue delays cellular senescence and enhances key mitochondrial biochemical pathways. *FASEB J.* **22**, 703–712 (2008).
13. Lee, K. K. & Boelsterli, U. A. Bypassing the compromised mitochondrial electron transport with methylene blue alleviates efavirenz/isoniazid-induced oxidant stress and mitochondria-mediated cell death in mouse hepatocytes. *Redox Biol.* **2**, 599–609 (2014).
14. Schmitz, O. *et al.* Molecular Biological Analysis of a Bidirectional Hydrogenase from Cyanobacteria. *Europ. J. Biochem.* **233**, 266–276 (1995).
15. Aubert-Jousset, E., Cano, M., Guedeney, G., Richaud, P. & Cournac, L. Role of HoxE subunit in *Synechocystis* PCC6803 hydrogenase. *FEBS Journal* **278**, 4035–4043 (2011).
16. Gutekunst, K. *et al.* The bidirectional NiFe-hydrogenase in *Synechocystis* sp. PCC 6803 Is reduced by flavodoxin and ferredoxin and is essential under mixotrophic, nitrate-limiting conditions. *JBC* **289**, 1930–1937 (2014).
17. Schneider, K. & Schlegel, H. G. Purification and properties of Soluble Hydrogenase from *Alcaligenes eutrophus* H16. *Cell* **452**, 66–80 (1976).
18. Van Der Linden, E. *et al.* Selective release and function of one of the two FMN groups in the cytoplasmic NAD^+-reducing [NiFe]-hydrogenase from *Ralstonia eutropha*. *Europ. J. Biochem.* **271**, 801–808 (2004).
19. Hagen, W. R. *Biomolecular EPR Spectroscopy*. (CRC press, 2009).
20. Rupp, H., Rao, K., Hall, D. & Cammack, R. Electron spin relaxation of iron-sulphur proteins studied by microwave power saturation. *Biochim. Biophys. Acta* **537**, 255–269 (1978).
21. Hirsh, D. J. & Brudvig, G. W. Measuring distances in proteins by saturation-recovery EPR. *Nat Protoc* **2**, 1770–1781 (2007).
22. Uhlmann, M. & Friedrich, T. EPR signals assigned to Fe/S cluster N1c of the *Escherichia coli* NADH:Ubiquinone oxidoreductase (complex I) derive from cluster N1a. *Biochem.* **44**, 1653–1658 (2005).
23. Reda, T., Barker, C. D. & Hirst, J. Reduction of the iron-sulfur clusters in mitochondrial NADH:ubiquinone oxidoreductase (complex I) by EuII-DTPA, a very low potential reductant. *Biochem.* **47**, 8885–8893 (2008).
24. Yano, T., Sled, V. D., Ohnishi, T. & Yagi, T. Expression and characterization of the flavoprotein subcomplex composed of 50-kDa (NQO1) and 25-kDa (NQO2) subunits of the proton-translocating NADH-quinone oxidoreductase of *Paracoccus denitrificans*. *JBC* **271**, 5907–5913 (1996).
25. Duffus, B. R., Gauglitz, M., Teutloff, C. & Leimkühler, S. Redox potentials elucidate the electron transfer pathway of NAD^+-dependent formate dehydrogenases. *J. Inorg. Biochem.* **253**, 112487 (2024).
26. Germer, F. *et al.* Overexpression, isolation, and spectroscopic characterization of the bidirectional [NiFe] hydrogenase from *Synechocystis* sp. PCC 6803. *JBC* **284**, 36462–36472 (2009).
27. Preissler, J. *et al.* Enzymatic and spectroscopic properties of a thermostable [NiFe]-hydrogenase performing H_2-driven NAD^+-reduction in the presence of O_2. *Biochim. Biophys. Acta - Bioenerg.* **1859**, 8–18 (2018).
28. Serebryakova, L. T., Medina, M., Zorin, N. A., Gogotov, I. N. & Cammack, R. Reversible Hydrogenase of *Anabaena variabil* ATCC 29413 Catalytic Properties and Characterization of Redox Centres. *BS 16842 FEBS Letters* vol. 383 (1996).
29. Bryant, F. O. & Adams, M. W. Characterization of hydrogenase from the hyperthermophilic archaebacterium, *Pyrococcus furiosus*. *J Biol Chem* **264**, 5070–5079 (1989).
30. Jumper, J. *et al.* Highly accurate protein structure prediction with AlphaFold. *Nature* **596**, 583–589 (2021).
31. Evans, R. *et al.* Protein complex prediction with AlphaFold-Multimer. *bioRxiv - Preprint* (2021) doi:10.1101/2021.10.04.463034.
32. Hekkelman, M. L., de Vries, I., Joosten, R. P. & Perrakis, A. AlphaFill: enriching AlphaFold models with ligands and cofactors. *Nature Meth.* **20**, 205–213 (2023).
33. Waterhouse, A. *et al.* SWISS-MODEL: homology modelling of protein structures and complexes. *Nucleic Acids Res.* **46**, W296–W303 (2018).
34. DeLano, W. L. PyMOL: An open-source molecular graphics tool. *CCP4 Newsl. Protein Crystallogr.* **40**, 82–92 (2002).
35. Peters, J. W., Lanzilotta, W. N., Lemon, B. J. & Seefeldt, L. C. X-ray crystal structure of the Fe-only hydrogenase (CpI) from *Clostridium pasteurianum* to 1.8 angstrom resolution. *Science* **282**, 1853–8 (1998).
36. Sazanov, L. A. & Hinchliffe, P. Structure of the Hydrophilic Domain of Respiratory Complex I from *Thermus thermophilus*. *Science (1979)* **311**, 1430–1436 (2006).
37. Radon, C. *et al.* Cryo-EM structures reveal intricate Fe-S cluster arrangement and charging in *Rhodobacter capsulatus* formate dehydrogenase. *Nature Comm.* **11**, 1–9 (2020).
38. Van Den Heuvel, R. H. H. *et al.* The active conformation of glutamate synthase and its binding to ferredoxin. *J. Mol. Biol.* **330**, 113–128 (2003).

39. Yan, Y., Tao, H., He, J. & Huang, S. Y. The HDOCK server for integrated protein–protein docking. *Nat. Protoc.* **15**, 1829–1852 (2020).
40. Huang, S. Y. & Zou, X. An iterative knowledge-based scoring function for protein-protein recognition. *Proteins: Struct. Funct. Genet.* **72**, 557–579 (2008).
41. Yan, Y., Zhang, D., Zhou, P., Li, B. & Huang, S. Y. HDOCK: A web server for protein-protein and protein-DNA/RNA docking based on a hybrid strategy. *Nucleic Acids Res.* **45**, W365–W373 (2017).
42. Page, C. C., Moser, C. C., Chen, X. & Dutton, P. L. Natural Engineering Principles of Electron Tunneling in Biological Oxidation-reduction. *NATURE* vol. 402 (1999).
43. Reece, S. Y., Hodgkiss, J. M., Stubbe, J. A. & Nocera, D. G. Proton-coupled electron transfer: The mechanistic underpinning for radical transport and catalysis in biology. in *Philos. Trans. R. Soc. Lond., B, Biol. Sci.* vol. 361 1351–1364 (Royal Society, 2006).
44. Barry, B. A. Reaction dynamics and proton coupled electron transfer: Studies of tyrosine-based charge transfer in natural and biomimetic systems. *Biochim. Biophys. Acta - Bioenerg.* **1847**, 46–54 (2015).